ANZIAM J. 52(2011), 225–249
doi:10.1017/S1446181111000733

THE MECHANICS OF HEARING: A COMPARATIVE CASE STUDY IN BIO-MATHEMATICAL MODELLING

A. R. CHAMPNEYS ✉[1], D. AVITABILE[2], M. HOMER[1] and R. SZALAI[1]

(Received 10 June, 2011; revised 30 July, 2011)

Abstract

A synthesis is presented of two recent studies on modelling the nonlinear neuro-mechanical hearing processes in mosquitoes and in mammals. In each case, a hierarchy of models is considered in attempts to understand data that shows nonlinear amplification and compression of incoming sound signals. The insect's hearing is tuned to the vicinity of a single input frequency. Nonlinear response occurs via an arrangement of many dual capacity neuro-mechanical units called scolopidia within the Johnston's organ. It is shown how the observed data can be captured by a simple nonlinear oscillator model that is derived from homogenization of a more complex model involving a radial array of scolopidia. The physiology of the mammalian cochlea is much more complex, with hearing occurring via a travelling wave along a tapered, compartmentalized tube. Waves travel a frequency-dependent distance along the tube, at which point they are amplified and "heard". Local models are reviewed for the pickup mechanism, within the outer hair cells of the organ of Corti. The current debate in the literature is elucidated, on the relative importance of two possible nonlinear mechanisms: active hair bundles and somatic motility. It is argued that the best experimental agreement can be found when the nonlinear terms include longitudinal coupling, the physiological basis of which is described. A discussion section summarizes the lessons learnt from both studies and attempts to shed light on the more general question of what constitutes a good mathematical model of a complex physiological process.

2010 *Mathematics subject classification*: primary 34C23; secondary 92C30, 74H45, 74J30.

Keywords and phrases: mathematical biology, hearing, dynamical systems.

1. Introduction

This article surveys, compares and contrasts recent work by the authors and their co-workers on two distinct mathematical modelling problems: attempts to understand

[1]Department of Engineering Mathematics, University of Bristol, Bristol, BS8 1TR, United Kingdom; e-mail: a.r.champneys@bristol.ac.uk, martin-homer@bristol.ac.uk, r.szalai@bristol.ac.uk.
[2]Department of Mathematics, University of Surrey, Guildford, GU2 7XH, United Kingdom; e-mail: D.Avitabile@surrey.ac.uk.

the highly developed hearing of mosquitoes and the corresponding process within the mammalian ear. The two problems share certain features. In particular, there is a transduction from sound pressure waves in air into neural signals. Moreover, both involve active, nonlinear mechanical amplification that applies to certain input sound frequencies and amplitudes. However, there are also huge differences.

The insect "design solution" is remarkably simple: there is an almost direct transduction. The motion of the external organ (the antenna) feeds directly into individual mechano-sensitive units called scolopidia. Each scolopidium contains a single neuron that transmits signals directly to the brain, and there is no further neural processing of the sound. In addition, the scolopidia contain dynein molecules that are able to transmit a force back to the antenna, causing active amplification. See Section 2 below for more details of the physiology.

In contrast, mammalian hearing is far more complex; see Section 3 for details. Quite apart from the many levels of neural processing that occur in the brain, the mechanical part of sound reception occurs via the interaction of many embedded structures and processes. Specifically, air pressure waves are converted by the middle ear into fluid–structure interaction waves inside the coiled cochlear tube. The main stiff element inside the tube is the basilar membrane (BM). Vibrations of the BM are measured by the so-called organ of Corti (OC), a transverse structure resting on the BM that is replicated longitudinally along the tube: different longitudinal positions correspond to distinct frequencies. Within the OC there are two kinds of mechano-sensory cells: the inner hair cells and outer hair cells (OHCs). The inner hair cells are responsible for transduction of the mechanical vibrations into neural pulses that are passed along the aural nerve to the brain. The main function of the outer hair cells appears to be that of selective mechanical amplification of the vibrations in order to enhance frequency tuning. The process by which this amplification occurs is far from clear and is the subject of current debate in the literature.

First and foremost, this article serves to elucidate by mathematical modelling the relative merits of the insect and mammalian hearing organs. Both have remarkable sensitivity to low sound levels, but, whereas the insect has highly accurate direction sensitivity, mammals have remarkable ability to differentiate frequencies. There is, though, a second aim to this article: to seek answers to the question of what is a "good" mathematical model in the life sciences.

In the physical sciences, the laws of physics generally lead to well-established mathematical theories. There are incontestable mathematical models, such as the Navier–Stokes equations for fluid flow or the theory of finite strain elasticity for solid deformation. The state of the art appears to be the variety of methods by which these models are studied: simulation, asymptotic analysis, rigorous existence theory, and so on. As applied mathematics moves into the second decade of the new millennium, however, increasingly our discipline is being asked to contribute to the social and life sciences. What might represent a good model in the social sciences, or indeed whether modelling really has the same meaning in systems that involve human behaviour "in the loop", remains a philosophical and metaphysical challenge for our community. We

do not attempt to enter that debate here. In the life sciences, however, it would seem timely to contribute observations pertinent to the philosophy of modelling, using the biological systems studied here as illustrations.

The rest of this paper is outlined as follows. Sections 2 and 3 contain results on the modelling of insect and mammalian hearing respectively. In both cases we briefly explain the anatomy and present some existing physiological experimental recordings. For each, we review a hierarchy of mathematical models that attempt to explain the data. The paper is brought to a close by a discussion in Section 4 that attempts to draw out the more general conclusions from these modelling case studies.

2. Antennal hearing in insects

Insects have evolved diverse and delicate morphological structures in order to capture the inherently low energy of a propagating sound wave. In mosquitoes, which have one of the most highly evolved hearing systems within the insect kingdom, an active process occurs within the pair of Johnston's organs, located at the base of each antenna. Within this organ, the capture of acoustic energy and its transduction into neuronal signals is assisted by the active mechanical participation of so-called *scolopidia*, which combine neuron activation with dynein-activated mechanical response. The Johnston's organ has 120-fold rotational symmetry, allowing a high degree of direction sensitivity. For this work, though, we assume that incoming sound comes from a single well-defined direction, and so consider the physiology within a single radial slice; see Figure 1. The active process that takes place within the male Johnston's organ was first described by Gopfert and Robert [16]; see also Jackson and Robert [22]. The process involves amplification, and subsequent compression, with increased sound pressure levels of near-resonant frequencies (tuned to that of the female wingbeat), and shows significant hysteresis for sub-resonant frequencies; see Figure 2 for typical experimental recordings.

2.1. A phenomenological model The first attempt to mathematically explain the dynamics of this active process was due to Jackson et al. [23]. They posed a coupled Ginzburg–Landau-like model

$$\frac{dR}{dt} = (-\gamma - i\Delta)R + iF, \tag{2.1}$$

$$\frac{dA}{dt} = a_1 A + a_2|A|^2 A + R\overline{A} \tag{2.2}$$

for the complex amplitude of the antennal motion $R(t)$, which responds to an input sound $F(t) = F_0 e^{i\omega t}$, and a spatially homogeneous variable $A(t)$ describing the force provided by the collection of scolopidia in one radial slice. Here γ, Δ, a_1 and a_2 are generic fitting parameters and an overline represents complex conjugation. With suitable choices of these parameters, good agreement is found with experimental data, including the presence of hysteresis upon variation of input amplitude for mildly subcritical frequencies ω (the corresponding experimental data is presented in Figure 2

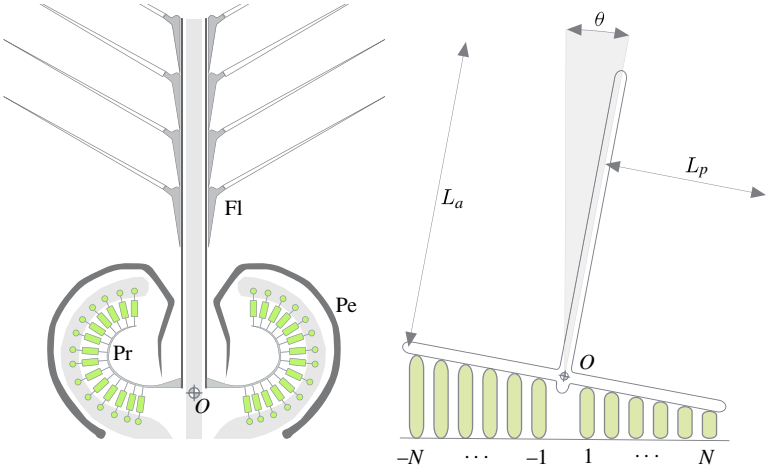

FIGURE 1. Morphology of the auditory organ of the mosquito species *Toxorhynchites brevipalpis*. Left: schematic section of the antenna and of the Johnston's organ. The male flagellum (Fl) bears numerous hairs and its base is implanted in the pedicel (Pe). The pedicel encloses a set of mechano-sensory neurons (scolopidia), attached to a stiff prong (Pr). The main mode of vibration of the antenna is a rigid in-plane rotation around *O*. Right: sketch of the integrate-and-twitch model (not to scale). The flagellum and prong are merged into one rigid body, while ensembles of scolopidia are modelled by compound objects called *threads*. Antennal rotations induce thread compressions and extensions.

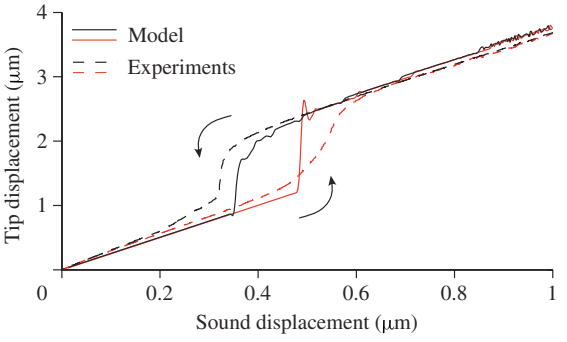

FIGURE 2. Nonlinear amplification and hysteresis in the antennal displacements of the mosquito species *Toxorhynchites brevipalpis*. The specimen is subject to a controlled sound field which is first increased (lower curves) and then decreased (upper curves) quasi-statically. The picture shows a comparison between experiments (dashed lines) and numerical simulations of the integrate-and-twitch model (solid lines). Figure adapted from Avitabile et al. [3].

below). However, the model (2.1) and (2.2) is in some sense merely descriptive in that it is hard to ascribe physical meaning to the parameters or to understand the physiological origins of the nonlinear terms.

In this paper we present two further mathematical models whose purpose is to be predictive. The first attempts to capture the physiology at a more meso-scale, via a description of the mechanistic response of the scolopidia as a process of integration

of ionic currents up to a threshold. At such a threshold the scolopidium is assumed to "twitch", that is, to provide a mechanical force back to the radial "prong" that is attached rigidly to the antenna's pedestal. The ion channels of the scolopidium are assumed to open under sufficient compression, that is, after sufficient angular displacement of the antenna. For ease of computation, we do not generally include an anatomically correct number of scolopidia in our simulation. Instead, we assume that a number of scolopidia are bundled together in coarse-lump units, or *threads* whose parameters are correctly scaled to represent the correct overall amount of force on the radial prong. The second model then attempts to homogenize this micro-scale model into a macro-scale nonlinear oscillator that averages the combined response of all the scolopidia into an effective active nonlinear substrate to which the antenna is anchored.

2.2. The integrate-and-twitch model The *integrate-and-twitch* model was introduced by Avitabile et al. [3] and can be compactly written as

$$\ddot{\theta} + c\dot{\theta} + k\theta = \frac{1}{J}(M_{\mathrm{s}}(t) + M_{\mathrm{t}}(\mathbf{n})), \quad \dot{\mathbf{n}} = -l_1\mathbf{n} + l_2\mathbf{G}(\theta, \mathbf{n}). \tag{2.3}$$

Here the antenna, whose angular displacement is denoted by θ, is modelled as a damped oscillator subject to an external forcing. The forcing consists of two contributions: the external sound field, M_{s}, and the mechanical action of the threads, M_{t}. The vector $\mathbf{n}$ collects the thread potentials, whose time evolution is ruled by two competing effects: a charge at rate proportional to the parameter l_2, and a discharge at rate proportional to l_1. The threads are coupled to the antennal displacements via the vector-valued function $\mathbf{G}$, whose ith component can assume only two values: 1 if the ith thread is charging, or 0 if the ith thread is not charging.

To close the model, we need expressions for M_{s}, M_{t} and $\mathbf{G}$. The impinging sound field can be modelled in general as a Fourier series, but for simplicity, in this study we consider the response to a single harmonic. Therefore we have

$$M_{\mathrm{s}}(t) = X_{\mathrm{s}} \cos(\omega_{\mathrm{s}} t). \tag{2.4}$$

The moment exerted on the antenna by the threads is assumed to be given by a series of impulsive torques

$$M_{\mathrm{t}}(\mathbf{n}) = \sum_{i=-N}^{N} m_i(n_i) = \sum_{i=-N}^{N} \sum_{j=1}^{\infty} fi(\Delta a)\delta(t - t_{ij}(n_i)), \tag{2.5}$$

where the threads are numbered from $-N$ to N and assumed to be uniformly distributed along an antennal prong, at a fixed separation distance Δa, and δ is the Dirac delta function. The ith thread twitches when its potential n_i reaches a given threshold. This twitching may occur several times per cycle of antenna oscillation, so we keep a generation notation $t_{ij}(n_i)$ for the time instant at which the ith thread twitches for the jth time. With reference to the system (2.3), we define implicitly t_{ij} as the time for which $n_i(t_{ij}) = h$. When a thread twitches, (2.5) states that it provides an impulse

force f with a lever arm $i\Delta a$; also, the thread resets to zero and remains inactive for a refactory period d.

The coupling of the threads to the antenna, $\mathbf{G}$, is expressed using suitably defined Heaviside functions:

$$G_i(\theta, n_i) = H(i\theta(\Delta a) - s)\Big(1 - \sum_{j=1}^{\infty} H(t - t_{ij}(n_i)) - H(t - t_{ij}(n_i) - d)\Big). \tag{2.6}$$

In other words, the ith thread is allowed to charge if two conditions are met: first, the antennal displacement θ must induce a compression $i\theta\Delta a$ larger than the threshold s; second, a refactory time d must have passed since the last twitch.

The integrate-and-twitch model reproduces several nonlinear mechanical features found in experiments on the mosquito species *Toxorhynchites brevipalpis*. Figure 2 shows a comparison between the model predictions and the experimental results. Parameter choices are the same as those used by Avitabile et al. [3], which were as far as possible derived from physiological estimates rather than from a posteriori data fitting. In the experiment, the amplitude of the antennal oscillations is recorded when the specimen is subject to a controlled sound field at fixed frequency ($\omega_s \approx 2\pi \cdot 400$ rad s^{-1}) and variable amplitude X_s. The parameter X_s is varied quasi-statically during the experiment: it is first increased linearly along the lower curve, and then decreased along the upper curve. The antennal response features both nonlinear amplification and hysteresis, which are captured by the model.

Further experimental agreement for different input frequencies was presented in the work of Avitabile et al. [3], as well as suggestive evidence that the timing of the charging and subsequent twitching of the scolopidial threads is consistent with the neural transmission signal. Furthermore, it was shown how the model can capture the phenomenon of spontaneous oscillations that are observed in some individuals.

2.3. A continuum limit The schematic diagram in Figure 4 shows that the mechanical effect of the scolopidia is to provide a nonlinear forcing when the antennal displacement is above a critical value θ_c (where $\theta_c \approx 0.3$ in the simulations presented thus far). This suggests that it should be possible to re-interpret the integrate-and-twitch model as a simple nonlinear oscillator

$$\ddot{\theta} + c\dot{\theta} + k\theta + f_{\mathrm{ho}}(\theta, \dot{\theta}) = \frac{1}{J} M_s(t) \tag{2.7}$$

for a suitably defined homogenized restoring force f_{ho}. Comparing (2.3) and (2.7), we see that in the new formulation there is no equation for each thread's potential. Instead, we homogenize the mechanical action of all threads via the nonlinear function f_{ho}, which in general should depend directly on the angular displacement and velocity.

The main new result presented here is to announce that it is possible to pass from the *discretized model* (2.3)–(2.6) to the *continuum model* (2.7) via a process of nonlinear averaging. The details will be presented elsewhere. The key is to introduce a discrete set of angles $n\Delta\theta$, $n = -N, \ldots, N$ and average the force provided by the scolopidia

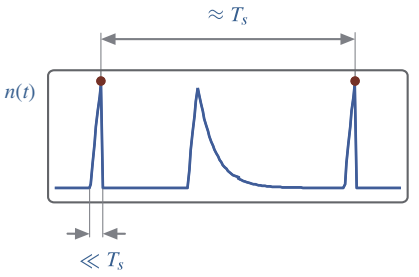

FIGURE 3. A time profile of a thread potential in the integrate-and-twitch model. The charging time is usually much shorter than the period of the impinging sound and the threads twitch typically once per period (twitches are denoted with dots).

as the angle is increased (or decreased) from θ to $\theta + \Delta\theta$. The continuum model is obtained by carefully taking the limit $\Delta\theta \to 0$ and $\Delta a \to 0$, that is $N \to \infty$, under certain approximating assumptions.

The main assumptions concern the relative time scales of charging and refactoriness in each scolopidium. Figure 3 shows the time profile of thread potentials, obtained by simulating the discrete model with $N = 20$ and $X_s = 0.6$ μm. The characteristic charging time is typically much smaller than the period of the external sound field, T_s, and the time between two consecutive twitches is approximately T_s. Therefore, if we want to account only for the mechanical action of the threads, it makes sense to disregard what happens between two twitches and assume that the threads twitch once per period, as soon as their compression thresholds $\theta_i = s/(i\Delta a)$ are reached (see (2.6)).

To homogenize, focus on the twitching sequence occurring when $\theta > \theta_c > 0$ and $\dot\theta > 0$ (see the sketch in Figure 4). Without loss of generality, assume that thread P (with $P < N$) twitches when the antenna has angular displacement θ. Then the antenna continues to move, accelerated by the external sound field and the impulsive momentum just provided by P, thus allowing more threads to twitch. When the antennal displacement is $\theta + \Delta\theta$, thread Q twitches. Between θ and $\theta + \Delta\theta$, we count $P - Q$ twitches. The average momentum between θ and $\theta + \Delta\theta$ is then

$$\begin{aligned}\langle M_t\rangle &= \frac{\dot\theta}{\Delta\theta}\int_\theta^{\theta+\Delta\theta}\sum_{i=Q}^{P}(b\Delta a)(i\Delta a)\delta(\varphi-\theta_i)\,d\varphi = \frac{b\dot\theta\Delta a^2}{\Delta\theta}\sum_{i=Q}^{P} i \\ &= \frac{b\dot\theta\Delta a^2}{\Delta\theta}\left(\frac{P^2-Q^2+P+Q}{2}\right) \\ &= \frac{b\dot\theta}{2}\left(\frac{s^2}{\theta^2\Delta\theta}+\frac{s\Delta a}{\theta\Delta\theta}-\frac{s^2}{(\theta+\Delta\theta)^2\Delta\theta}+\frac{s\Delta a}{(\theta+\Delta\theta)\Delta\theta}\right).\end{aligned} \tag{2.8}$$

It is instructive to compare the active torque in the discrete and in the continuum model (respectively, equations (2.5) and (2.8)). In the derivation of the average moment $\langle M_t\rangle$, we have expressed the impulsive force as $f = b\Delta a$, so that the

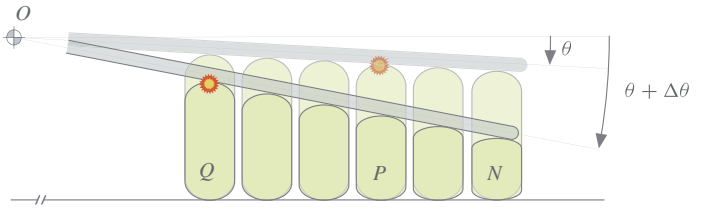

FIGURE 4. Twitches between angles θ and $\theta + \Delta\theta$. Thread P twitches when the antenna has angular displacement θ. The antenna continues to move, sustained by both the external sound field and the impulsive twitch just provided by P. This allows more threads to twitch. When the antennal displacement is $\theta + \Delta\theta$, thread Q twitches. Between θ and $\theta + \Delta\theta$, we count $P - Q$ twitches.

contribution of a single thread tends to zero as $\Delta a \to 0$, as expected. In addition, we have used our assumptions on the thread dynamics: first, we have only one twitch per period, so there is no sum over j; second, the threads fire instantly when they reach their compression thresholds, and therefore twitching times t_i translate naturally into twitching angles θ_i (the change of variables results in the factor $\dot{\theta}$ in front of the integral); and finally, twitching angles are related to angular displacements via simple geometric equations, in particular

$$\theta = \theta_P = \frac{s}{P\Delta a}, \quad \theta + \Delta\theta = \theta_Q = \frac{s}{Q\Delta a},$$

which have been used to obtain the last expression of (2.8).

We now proceed to take the limit of the average moment $\langle M_t \rangle$ for $\Delta\theta \to 0$ and $\Delta a \to 0$. We pose $\Delta\theta = \varepsilon$ and assume that when the antenna spans the small angular displacement $\Delta\theta$, a large number of threads become active and fire, that is, $\Delta a/\Delta\theta = O(\varepsilon)$, or equivalently $\Delta a = O(\varepsilon^2)$. We then find

$$\lim_{\varepsilon \to 0} \langle M_t \rangle = \frac{bs^2\dot{\theta}}{\theta^3},$$

which gives us the desired expression for the homogenized nonlinearity $f_{ho}(\theta, \dot{\theta})$:

$$f_{ho}(\theta, \dot{\theta}) = \begin{cases} -bs^2\dot{\theta}/\theta^3 & \text{if } \theta > \theta_c \text{ and } \dot{\theta} > 0, \\ bs^2\dot{\theta}/\theta^3 & \text{if } \theta < -\theta_c \text{ and } \dot{\theta} < 0, \\ 0 & \text{otherwise.} \end{cases} \tag{2.9}$$

Interestingly, this nonlinearity has a striking similarity with the slow–fast nonlinearity of the van der Pol oscillator [17], as opposed to the Hopf-like nonlinearity in (2.2).

Let us now compare the two models. On one hand, we have the discrete model (2.3)–(2.6), which will be run for large but finite N; on the other hand, we have the continuum model (2.7), whose nonlinearity is given by (2.9). The models share the same parameters for the sound field, antennal stiffness/damping and thread impulse. A first comparison is shown in Figure 5. In this numerical experiment, we fix $X_s = 0.6\,\mu$m

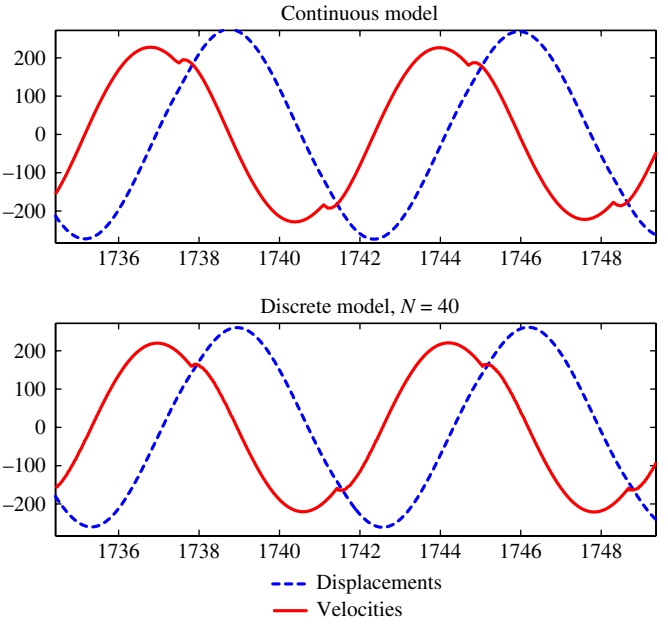

FIGURE 5. Comparison between the continuous model (top) and the discrete model with $N = 40$, corresponding to 80 threads (bottom). In both models, the external sound field has amplitude $X_s = 0.6\,\mu$m. For each model, we show dimensionless displacements (dashed line) and velocities (solid line). The effect of the threads can be seen in the velocity profiles. In the continuous model, the sudden changes in velocities are provided by the averaged nonlinearity (2.9); in the discrete model, the changes in velocities are due to the thread twitches (2.5).

and show that the two models have similar dimensionless displacements and velocities. The effect of the threads is best seen in the velocity profiles: in the continuum model, the sudden changes in velocities are provided by the averaged nonlinearity (2.9); in the discrete model, the changes in velocities are due to the thread twitches (2.5).

It is also interesting to see how the continuum model behaves when the intensity of the sound field is varied quasi-statically, as in Figure 2. The results of this test are collected in Figure 6, comparing the continuum model with the discrete model, for $N = 4, 8, 16, 32, 64, 128$. For the discrete model, we plot only the curves relative to a linearly increasing forcing and show how these curves accumulate as $N \to \infty$. We then pass to the continuum model, for which we plot the curve relative to both increasing and decreasing forcing, showing that this model also supports hysteresis. Note that the sharp rise in the increasing case almost overlays the discrete model results, whereas the sudden drop upon decreasing input levels occurs for much lower values.

3. Mammalian cochlear mechanics

In contrast to insect hearing, mammalian hearing is a complex process, composed of many highly developed sub-systems. The outer ear has a purely acoustic function. In

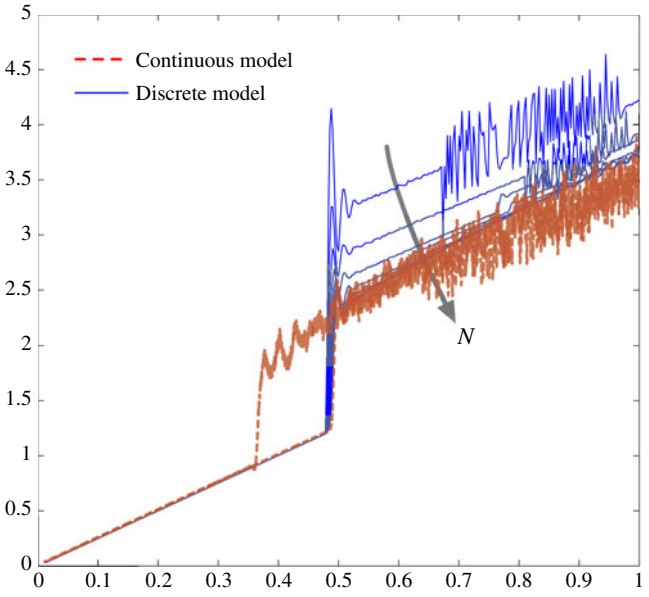

FIGURE 6. Comparison between the continuous model (dashed line) and the discrete model (solid line) when the amplitude of the external sound field is varied quasi-statically, as in Figure 2. For the discrete model, we repeat the simulation for several values of $N = 2, 4, 8, 16, 32, 64, 128$. See text for details.

the middle ear, the three small bones — the *malleus*, *incus* and *stapes* — are essentially there to match the impedance of sound waves in the outside air to that of waves in the fluid-filled cochlea. The cochlea is widely held to contain the nonlinear, active component of the auditory system, and its main function is to convert sound-evoked fluid motions into neural signals.

The cochlea is a remarkable organ. It is primarily a coiled tube filled with perilymph fluid whose purpose is to transduce sound pressure waves into neural signals. Each longitudinal position is sensitive to a specific frequency, which provides the basis for the sharp ability to differentiate nearby frequencies. In addition, the living cochlea performs quite advanced electromechanical pre-processing of sound. Specifically, active processes enable about 60 dB mechanical amplification of vibrations of the basilar membrane (BM) which longitudinally divides the cochlear tube. This amplification is nonlinear: six magnitudes of input sound pressure variations are compressed into three magnitudes of mechanical vibrations. These active processes also significantly enhance frequency tuning.

Figure 7(a, b) shows a schematic view of the cochlea. It is a coiled tube consisting of three fluid-filled chambers: the *scala tympani*, *scala media* and *scala vestibuli*. At the basal end there are two openings: the oval window, which is connected to the middle ear, and the round window, which is covered by an elastic membrane. The scala tympani and scala media are separated by the *organ of Corti* (OC), which is

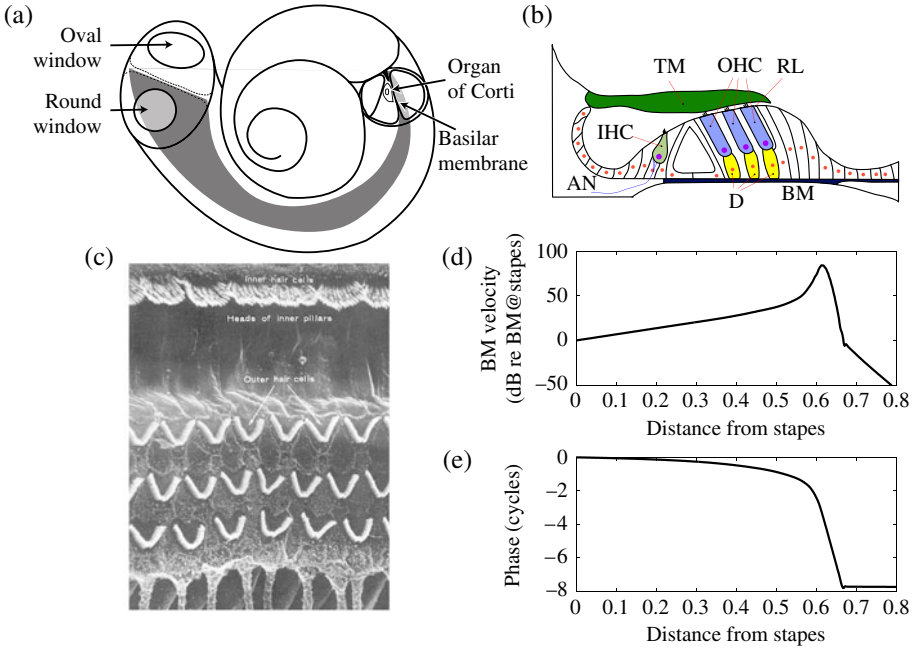

FIGURE 7. (a) Schematic view of the anatomy of the cochlea. (b) Schematic transverse section through the organ of Corti. Here TM represents the tectorial membrane, OHC an outer hair cell, RL the reticular lamina, BM the basilar membrane, D a Dieters cell, AN an auditory nerve and IHC an inner hair cell. (c) An image showing the arrangement of hair bundles of OHCs protruding beyond the RL in a view from above, with the vertical axis representing the transverse direction and the horizontal axis representing the longitudinal direction. (d,e) Schematic representation of the amplitude and phase of a travelling wave with transverse distance along the BM. The scale in (d) represents decibels relative to the intensity at the input from the stapes.

built on the flexible *basilar membrane* (BM). The scala media and scala tympani are separated only by the thin *Reissner's membrane*, and are usually modelled as a single chamber.

Since the pioneering theory due to Helmholtz [18], and the experiments of Békésy [4], the so-called theory of tonotopy has been widely accepted. That is, every transverse cross-section of the cochlea is most sensitive to a particular frequency, the so-called characteristic frequency (CF) of that location. The tonotopy map is such that low frequencies excite the BM at apical positions along the cochlear tube, while high frequencies stimulate the basal end. Specifically, following stimulation by the stapes, the fluid–structure interaction of the cochlear tube causes a travelling wave to be set up. This wave reaches a maximum amplitude and rapidly attenuates at a frequency-dependent distance from the stapes, thus explaining the tonotopic map. Such behaviour can be reproduced theoretically via a dynamic interplay between the fluid in the cochlear duct and the BM, with stiffness that varies with longitudinal position [29, 30, 41].

However, this is far from the whole story, because the BM is itself nonlinear [7, 34]. Typical experimental results are given in Figure 9(b, c), which shows the BM response obtained by Rhode [33] for a chinchilla cochlea at the CF position of 9.1 kHz when subjected to a range of different pure tone frequencies of varying amplitude. These data represent the experimental results by which we benchmark the results of our models.

Note from Figure 9(b) how the BM response is always nearly linear (the dashed line has slope equal to one for reference on this log–log plot) for small stimulation. For frequencies near the CF, the response quickly gets compressed, almost to saturation levels, as the stimulation amplitude is increased. For yet higher stimulating amplitudes there is a tendency for the response to return to linearity. For frequencies that are smaller than the CF (for example, 0.7 kHz) the response is nearly linear, albeit significantly weaker overall. This is a purely passive response. Thus, the data at the CF for low sound pressure levels should be seen as highly amplified (by about 60 dB) from the purely linear response, whereas the nonlinear compression has the effect of compressing about 90 dB of sound pressure input into about 30 dB of vibrational output. These results can also be understood when looking at the shape of the travelling wave depicted in Figure 7(d), which represents the output for a single amplitude and frequency of stimulation. The spatial location corresponding to the CF in that figure can be identified by the large peak in the response. Returning to Figure 9(b), note that for higher frequencies (for example, 13 kHz) the response is again almost linear, although now it is even weaker still, due to the location in question being beyond the attenuation region of the travelling wave.

There is a growing literature on various attempts to model cochlea function, which we cannot do justice to in this brief paper. For a summary of the state of the art, the interested reader is referred to the proceedings of the highly influential "Mechanics of Hearing" series of conferences, the 11th of which was held in Williamstown, Massachusetts in July 2011. It is worth pointing out, though, that there is another phenomenon that is particularly amenable to *in vitro* experimental measures. These are so-called otoacoustic emissions (OAEs), which are acoustic waves that propagate back through the middle ear to the surrounding air. Indeed, some individuals have ears that constantly "sing" due to spontaneous OAEs at low pressure levels that can be measured with an external microphone. Also, the induced otoacoustic response to delta function-like click stimuli can be used as a diagnostic tool to probe the nonlinearity of the inner ear. For brevity, we do not deal with OAEs in any detail here, but subsequent work will show how the final model we present provides a credible explanation of OAEs.

3.1. Phenomenological models The active component of the auditory system is widely accepted to be located within the outer hair cells (OHCs) of the OC. These particular cells have two types of active process [8, 20]. The hair bundle on top of the cell is motile, hence it can exert force against the vibrating structures of the cochlea. For example, the experimental results of Kennedy et al. [26] show that direct mechanical stimulation of the hair bundles can result in a period of negative stiffness. On the other hand, it has been observed [6] that if OHCs are depolarized, they shorten.

Later it was discovered that a piezoelectric protein called *prestin* embedded within the lateral membrane of the OHC body, or soma, is responsible for this effect [39]. Prestin can expand and contract in response to changes in the cell potential, and makes the cell body change its shape. Both bundle adaptation and somatic motility can be stimulated by cochlear vibrations, through the mechanically sensitive ion channels found at the tips of the hairs.

There is currently debate in the literature on the relative importance of these two forms of motility in the active amplification process within mammalian hearing [9]. While somatic motility may seem more obvious from a mechanical point of view, amplification also occurs in lower organisms such as birds and reptiles, whose hair cells do not contain prestin but have rather more pronounced stereocilia. On the other hand, transmission to the BM motion is more straightforward with a somatic motility hypothesis; for example, Lagarde et al. [28] provide experimental evidence suggesting somatic motility alone is sufficient. It has been suggested that the action of prestin may be too slow, although it has been shown that somatic motility can work up to higher than audible frequencies [13].

A schematic of an OHC is shown in Figure 8(c). It has ion channels that are connected to adjacent hairs in the bundle through elastic fibres, that is, the tip links. The tip links are also presumed, as in nonmammalian hair cells, to be coupled to myosin motors that pre-tension the tip link, perhaps to the most sensitive state of the ion channels. The ion channels are not only mechanically sensitive, but also calcium sensitive. This provides a fast adaptation mechanism to tune the operating point [27]. The myosin motors are similarly calcium sensitive, that is, their force decreases with increasing calcium concentration.

The negative stiffness seen in these hair cells, together with spontaneous oscillations of the bundles observed in lower vertebrates such as bullfrogs, has led to the hypothesis that the hair cell can essentially be modelled as a nonlinear oscillator undergoing a Hopf bifurcation [11]. Hudspeth [20] presented a detailed review, including appealing evidence that a forced Hopf bifurcation normal form can give rise to a compressive nonlinearity and a possible explanation for OAEs and two-tone interference in hearing [24]. The utility of the simple Hopf normal form phenomenological model has been argued as evidence for the bundle-adaptation hypothesis for the origin of the cochlea nonlinearity. However, more recent mathematical models suggest that the observed behaviour can be best explained by a combination of both bundle adaptation and somatic motility; see the work of Ó Maoiléidigh and Jülicher [32] and Section 3.2 below for more details.

There have been many other explanations of the source of the active process in hearing; see the reviews by Hudspeth et al. [21] and Ashmore et al. [1]. Of particular note is the work of Zweig [40], who added a linear feedback term to a simple travelling-wave model of the BM. The results were found to reproduce the active response of the cochlea well. Steele and collaborators [14, 35] found similar results using a spatial feed-forward term within the travelling wave equation. A discussion and extension of these results forms the subject of Section 3.3 below.

3.2. A local nonlinear model In order to understand the possible physiological basis for the Hopf bifurcation hypothesis, Tinevez et al. [38] adapted a model of the myosin motor mechanism constructed by Assad and Corey [2] that can account for gating currents observed on a voltage-clamped cell, as well as the mechanical properties of the hair bundle in bullfrogs. The current through the ion channels is qualitatively similar to that illustrated in Figure 8(b). In particular, Tinevez et al. [38] adapted the model to describe mammalian hair bundle dynamics, based on the experimental data of Kennedy et al. [26] (essentially as represented in Figure 8(a, b) below). It was found that this model can indeed undergo a Hopf bifurcation.

Ó Maoiléidigh and Jülicher [32] incorporated this myosin motor dynamics in their unified ODE model of an OHC that includes the charge dynamics and linear coupling to all the structural elements in the cochlea cross-section. Recently, Szalai et al. [36] analysed a version of this model and various other simplified ODE models using bifurcation analysis. They found that the dynamics of the system contains many local bifurcations including saddle-node, cusp and Hopf bifurcations of the equilibrium state. They argued that the presence of a bifurcation per se is not the most important feature in order to reproduce the observed compressive nonlinear response. Rather, it is the form of the nonlinearity within the model.

We present here a simplified version of a model of the dynamics of the OC that captures what we believe to be the simplest ingredients that are consistent with physiological observations. The model is depicted schematically in Figure 8(d); more details are given by Szalai et al. [36]. The model includes adaptation due to hair bundle displacement and nonlinearity of the transduction current. The actual force to move the BM is exerted by the OHC's somatic motility. We assume an elastic and underdamped BM. The hair cells connect to the BM through the elastic Dieters cells on one hand, and are rigidly fixed to the reticular lamina, which provides a stationary frame. The passive OC mechanism is assumed to stimulate the hair bundle, which in our model does not exert any force.

We use a simplified approach to describe the transduction current I as a function of the hair bundle displacement. To keep a consistent notation with earlier models [32], we refer to the deflection of the tip link from its equilibrium position via an adaptation variable y_a. Specifically, we assume

$$\dot{y}_a = -\kappa(y_a - Z), \tag{3.1}$$

$$I = -P_{\mathrm{O}}(\Delta(\alpha y_a + \beta \dot{y}_a)), \tag{3.2}$$

where Z is the applied force on the hair bundle, the open probability function P_{O} is given by the Boltzmann function

$$P_{\mathrm{O}}(y) = \frac{1}{1 + e^{-y}},$$

and the induced current has been scaled to unity if the ion channels are fully open. In contrast to previous work, we do not include separate dynamics for the hair bundle

displacement y and the tip link y_a, as we assume that any adaptation via myosin motors merely serves to tune the operating point of the open probability function of the ion channels, rather than to vary dynamically during each oscillation. The choice of the argument of the open probability function was motivated by experimental results [26].

The behaviour of this model is illustrated in Figure 8(a, b). As in the experiments, we have stimulated the hair bundle in the model with step displacements of different magnitude (shown in Figure 8(a)). This results in peaks of the transduction current whose maximum value depends on the height of the stimulating step with the function P_{O}. When the stimulation is held constant, the current falls to almost zero, that is, the adaptation is nearly complete. This means that the transduction current is more a function of the hair bundle velocity than its position. We found that the values $\alpha = 0.1$ and $\beta = 1$ form a good fit with the experimental observations. The overall scale factor Δ controls the slope of P_{O} at equilibrium.

To include (3.1) and (3.2) as a feedback mechanism, we assume that the BM is modelled as a linear oscillator with natural frequency ω_0, the CF of the longitudinal position in question, and damping ratio ζ. This BM motion is supposed to be coupled to the OHC through the Dieters cells, that are again represented by a spring and a damper. We suppose that the spring and damping constants of this coupling are chosen so that the extension $l(t)$ of the OHC causes an additional force on the BM equivalent to a reduced restoring force $-f_1\omega_0^2 l$ and reduced damping $-2f_0\zeta\omega_0\dot{l}$.

The length $l(t)$ of the OHC is supposed to be controlled linearly by somatic motility. Specifically, the excess charge q in the hair cell is assumed to leak at rate γ and the hair cell is assumed to expand or contract from its equilibrium length l_0 in direct proportion to the excess charge. For simplicity, the units of the charge are chosen so that $l(t) = l_0 + q(t)$. The hair cell is charged by the transduction current. The hair bundle excitation is driven by the BM motion $z(t)$ and indirectly by the assumed sinusoidal pressure difference $p = F \sin \omega t$. Even though the indirect forcing by the pressure is small, its effect can be rather large due to the sensitivity of the hair bundle. A parameter ϵ is included to represent the relative importance of $p(t)$ on the motion of the BM, z, and on the deflection of the hair bundles, y_a.

Under the above assumptions, the governing set of equations for the dynamics of the OC is

$$\begin{aligned} \ddot{z} &= -2\zeta\omega_0(\dot{z} - f_0\dot{q}) - \omega_0^2(z - f_1 q) + \epsilon F \sin \omega t, \\ \dot{y}_a &= -\kappa(y_a - (z + F \sin \omega t)), \\ \dot{q} &= -\gamma q + P_{\mathrm{O}}(\Delta(\alpha y_a + \beta \dot{y}_a)) - P_{\mathrm{O}}(0). \end{aligned} \tag{3.3}$$

Note that the only nonlinearity is the open probability function P_{O}.

The bifurcation diagram of (3.3) can be seen in Figure 8(e). The white region is stable and bounded by a pitchfork bifurcation (horizontal line) and a Hopf bifurcation curve (diagonal line). Both bifurcations are supercritical, hence there is no additional dynamics of the unforced system in the stable region other than the equilibrium. We have found that within the white stability region, the system is rather robust

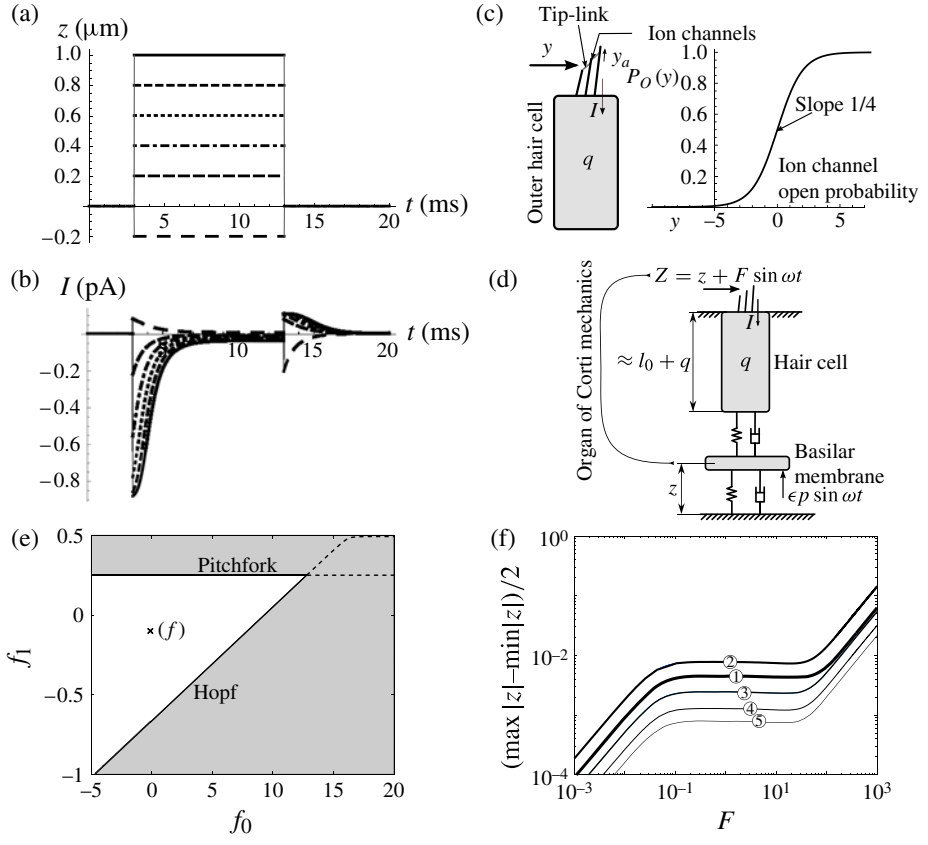

FIGURE 8. Outer hair cell active mechanisms: (a) applied hair bundle stimulation and (b) the corresponding transduction output current through the ion channels; (c) schematic depiction of the hair bundles and the outer hair open probability function; (d) schematic description of the overall mechanics. (e) Bifurcation diagram of the mathematical model (3.3) (see text for details) and (f) the mechanical response of the model at frequencies 5 kHz, 6.6 kHz, 8 kHz, 9 kHz and 10 kHz (labelled 1–5 respectively). Other parameter values used are $\alpha = 0.1$, $\beta = 1$, $\kappa = 6.6$, $f_0 = f_1 = -0.1$, $\omega_0 = 6.6 \times 2\pi$, $\zeta = 0.1$, $\epsilon = \gamma = 1/20$ and $\Delta = 8$.

to parameter changes. For our chosen set of parameters, denoted by a cross in Figure 8(e), the response of the model is shown in Figure 8(f). The response has the desired qualitative feature of being linear for small forcing amplitudes, compressive for medium amplitudes and linear again for higher amplitudes. One might notice that its tuning is rather sharp, sharper than is possible by a single degree of freedom (DOF) oscillator, but less sharp than a two DOF oscillator. This is due to the additional dynamics from the adaptation and charging of the hair cell.

The presence of a Hopf bifurcation within the bifurcation diagram of Figure 8(e), though, suggests a possible source of otoacoustic emissions as being due to the consequent limit cycle oscillation that might result from a perturbation to the system's

parameters away from its stable operating point. It has been suggested that spatial inhomogeneity in the cochlea might cause such a perturbation [12]. However, the Hopf bifurcation present in this cochlea model is more like a global than local feature of the hair bundle. In particular, it would seem strange from the point of view of *Occam's Razor* to believe that the OHCs represent an ensemble of critically tuned Hopf oscillators which also happen to have (almost) the same natural frequency as the BM at each longitudinal position. It would appear more natural to consider the combination of the OC and BM as a simple nonlinear oscillator which may exhibit a Hopf bifurcation as an emergent feature. In fact, as we outline in the next section, it is the nature of the longitudinal coupling between these oscillators that seems to be the most important feature in explaining experimental observations.

3.3. Longitudinal coupling The cochlea cannot simply be described as an ensemble of disconnected oscillators each subject to a simple pure-tone input. In truth, there is significant longitudinal coupling between individual OC cross-sections. Effects that cause this coupling include the longitudinal stiffness of the basilar membrane (which is significantly weaker than its transverse stiffness), the motion of the tectorial membrane, the fluid motion, the fact that the hair cells themselves tilt in the longitudinal direction, and that the Dieters cells are coupled longitudinally through so-called phalangeal processes (see Figure 9(a) for a schematic).

Early models of the cochlea assumed no coupling between basilar membrane cross-sections, other than the fluid motion in the ducts of the cochlea. These models could not account for every detail of the BM vibration, whether or not they included higher spatial dimensional fluid motion. On the other hand, Zweig [40] determined the impedance of the BM necessary to produce observed BM response. He found that the effective BM oscillator must have a negative damping coefficient and a linear time-delayed feedback term. Such a model is rather difficult to underpin physiologically. The negative damping could be thought of as a crude model of OHC cell dynamics, but there is no obvious physiological evidence for a local time delay in the OC of the appropriate duration.

The puzzle of Zweig however can be resolved by other means, for example that the longitudinal forward coupling mechanism in the cochlea can produce the same result [14, 35]. Recent work by Szalai et al. [37] provides further evidence in this direction, and an explanation of the similarities and differences between temporal delay and spatial feed-forward. Other forms of longitudinal coupling could arise from a second travelling wave [19] that could be related to either the tunnel of Corti flow [25] or the waves of the tectorial membrane [15]. Recently Meaud and Grosh [31] considered simple plate models for the BM and the tectorial membrane. They showed that the combined effects of these yield longitudinal coupling that is bi-directional. This bi-directional coupling was found to lead to a cochlea response that has broader, more realistic peaks and to lead to increased stability.

In this paper we use a combination of passive bi-directional coupling (as in the work of Meaud and Grosh [31]) and active forward coupling (as a more realistic surrogate

of the time delay in Zweig's model [37]). We then assume that the micro-mechanics is described by (3.3) with some simplifications.

Specifically, the model consists of two parts: the fluid dynamics in the chambers of the cochlea, and the micro-mechanical model of the OC. As is common in modelling the fluid mechanics, we assume an incompressible and inviscid fluid description of the perilymph, which yields a wave equation for the pressure difference p between the scala tympani and scala vestibuli, and the BM displacement z,

$$\frac{\partial^2 z}{\partial t^2}(x,t) = \frac{\epsilon^2}{m}\frac{\partial^2 p}{\partial x^2}(x,t). \tag{3.4}$$

Here the lumped parameter $\epsilon \approx 0.025$ is a function of the geometry of the cochlea chambers and the density of the perilymph fluid, while m is the mass surface density of the basilar membrane. We scale the cochlea length to unity; therefore $0 \le x \le 1$.

To describe the BM motion we use a simplified version of our local model (3.3). First, it is no longer necessary to introduce the applied forcing term $p = \sin(\omega_0 t)$ into the stimulation of the hair cells. Instead, we suppose that the BM (the main elastic member within the OC) drives all mechanical components within a cross-section, including the motion between the tectorial membrane and reticular lamina that stimulates the OHC hair bundles. Hence the variable Z can be replaced with something strictly proportional to the basilar membrane displacement z. Also, we assume that the current adaptation is rather fast compared to the other dynamics, that is, the adaptation variable y_a and the BM displacement z are also strictly proportional. Without loss of generality, we can assume $y_a = z$. The governing equations are thus

$$\begin{aligned}\frac{p(x,t)}{m} &= \ddot{z}(x,t) + 2\zeta\omega_0\dot{z}(x,t) + \omega_0^2(z(x,t) - f_b q(x - h(x),t)) \\ &\quad - \omega_0^2\frac{f_b}{2}(z(x - h(x),t) + z(x + h(x),t)), \\ \dot{q}(x,t) &= -\gamma q(x,t) + P_{\mathrm{O}}(\Delta(\alpha z(x,t) + \beta\dot{z}(x,t))) - P_{\mathrm{O}}(0).\end{aligned} \tag{3.5}$$

Another simplification to the model (3.3) is that we use only the charge q and not its derivative as the feed-forward term. However, we introduce feed-forward and feed-backward terms from the BM motion. These two terms are equal in magnitude, as they approximate the longitudinal stiffness of the BM, meaning that the membrane is more like an inhomogeneous elastic plate rather than an ensemble of strings [31]. For computational simplicity, we assume that the feed-forward distance $h(x)$ of the action of the hair cells is the same as the longitudinal coupling distance of the BM (although this assumption can easily be relaxed). A realistic estimate for the magnitude of $h(x)$ can be computed from the length of the hair cells based on the assumption that the geometry of the OC (Figure 9(a)) is self-similar at different positions along the length of the cochlea. Specifically, we take $h(x) = 1.2l(x)$, where l is the length of the OHC.

In order to match the experimental data of Rhode [33] reproduced in Figure 9(b,c), we assume the following mechanics for the BM: $l(x) = (0.0027 + 0.0027x)$,

natural frequency $\omega_0(x) = 2\pi \cdot 20.8(e^{-4.8354x} - 0.1455)$, and damping coefficient $\zeta(x) = 0.03(1 - e^{-40(1-x)}) + 0.1e^{-40(1-x)}$. We also include spatial inhomogeneity by assuming that the feedback coefficient f_b has a normal random distribution around $\bar{f}_b(x) = 0.08(1 - e^{-40(1-x)})$ with standard deviation $0.01\bar{f}_b(x)$. Other parameters are the same as in (3.3) with the exception of $\gamma = 1$.

We use a boundary-value problem formulation to solve (3.4) and (3.5). We also assume that the stapes is moved by a harmonic velocity, that is, $u(0, t) = A \sin \omega t$, where u is the fluid velocity of the scala vestibuli. From the one-dimensional fluid flow equation, we find that $\dot{u}(x, t) = -(1/\rho)p'(x, t)$, where ρ is the fluid density. Hence, assuming that the pressure at the cochlea apex vanishes, we find pressure boundary conditions

$$p'(0, t) = -\rho\omega A \cos \omega t, \quad p(1, t) = 0. \tag{3.6}$$

For the BM displacement z and charge q, since the response of the cochlea for a single tone excitation is periodic we prescribe a periodic boundary condition in time:

$$z(x, t) = z(x, t + \pi/\omega), \quad q(x, t) = q(x, t + \pi/\omega). \tag{3.7}$$

Preliminary numerical results are shown in Figure 9(d,e). More details will be presented elsewhere. The numerical method used to solve (3.4) and (3.5) subject to (3.6) and (3.7) is a finite-differences discretization in space and a piecewise-polynomial orthogonal collocation approximation in time [5]. The solution of the nonlinear equation is propagated with increasing forcing amplitude A using pseudo arc-length continuation [10].

Figure 9(b, c) shows, for comparison, Rhode's experimental results [33] at 9.1 kHz characteristic frequency (CF). Figure 9(b) shows the input–output functions for different stimulus frequencies. For frequencies substantially lower than CF, the response is linear. For frequencies closer to CF, the response becomes compressive for mid range amplitudes and tends towards linear for high amplitudes. The compressive nature remains for very high frequencies but the linear region for higher amplitudes starts earlier. In Figure 9(c), the cochlea response is shown as a function of frequency at constant amplitudes. For low amplitudes, the response has a distinct broad peak at the CF. With increasing amplitude, the peak gets less pronounced and slightly moves towards lower frequencies. The amplitude independent variation at lower frequencies observed in experiments could be due to the middle ear, while wiggles at higher than CF frequencies might be explained by interference of vibrations from the travelling wave and waves reflected back from disturbance along the cochlea. Another observation is that in Figure 9(c) the response at 13 kHz is nearly linear, even a little expansive. This might be explained by a second sound source, perhaps from the compressive wave or the BM longitudinally coupled dynamics.

The results of our model (3.4) and (3.5) are displayed in Figure 9(d,e). They are highly similar to the experimental results. The significant differences are that the numerical results show sharper responses, which yield somewhat thinner peaks in Figure 9(e), and curves that are somewhat further apart in Figure 9(d). Because

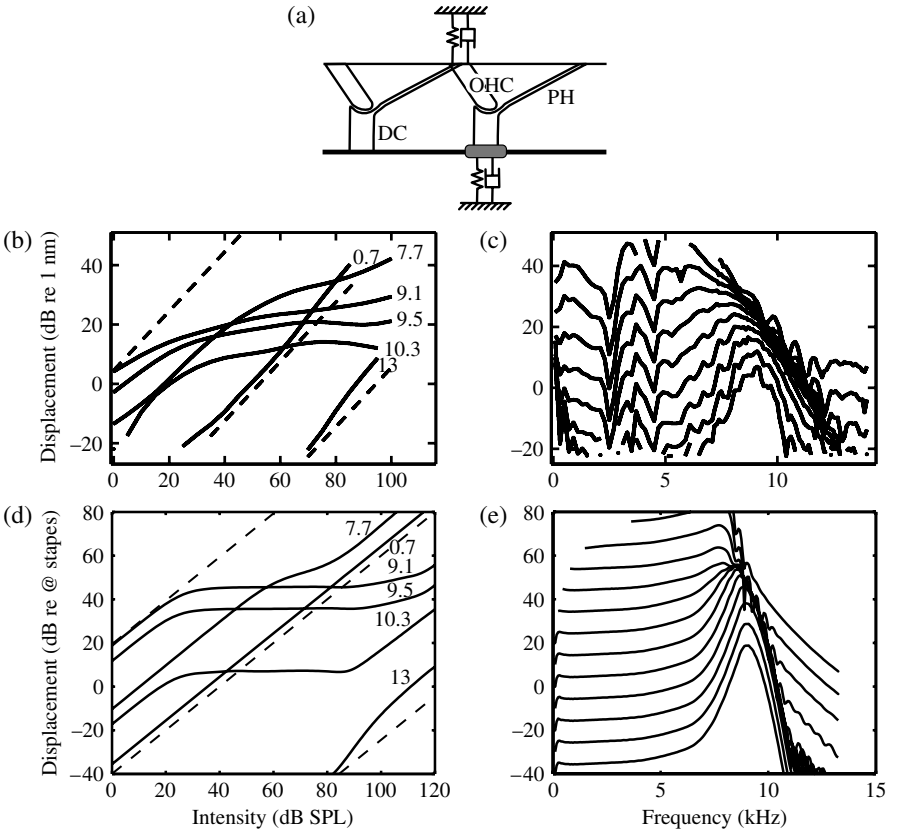

FIGURE 9. Models with longitudinal coupling. (a) Schematic diagram of a longitudinal cross-section of the organ of Corti. (b, c) Experimental data from Rhode [33] showing I/O functions measured on a chinchilla BM at CF = 9.1 kHz as a function of input amplitude and input frequency. The dashed lines have slope 1 for comparison. (d, e) Model predictions of (b) and (c) respectively. See text for details.

we do not model the middle ear, phase disturbances due to it (at low frequencies) are absent in Figure 9(e). However, the disturbances from the interference of the reflecting waves at high frequencies are reproduced in Figure 9(e). Also, perhaps surprisingly, in Figure 9(d) we get a similar response for the 13 kHz curve to the experimental result, showing early linearity for low enough sound pressure levels. An explanation for this might arise due to the longitudinal coupling, without which this curve would be flatter up until high-amplitude forcing. The exact mechanism for this linearity, however, is still under investigation.

4. Discussion

This paper has reviewed attempts to understand through mathematical modelling the nonlinear properties of the Johnston's organ in mosquitoes and the organ of Corti

in mammals. Each example has been a snapshot into ongoing research, and further results will appear elsewhere. Before undertaking a general comparison between the two studies, it is instructive to highlight some of the key features of each and to indicate future directions of research.

In the insect work, reviewed in Section 2, good quantitative agreement with experiments has been found for the integrate-and-twitch model, even over a range of input frequencies [3]. One benefit of this model over the earlier Ginzburg–Landau model is that each of its parameters has a clear physiological meaning and can be experimentally estimated. This modelling at a meso-scale has enabled us to scale up to a macro-scale model, essentially to estimate the homogenized nonlinearity provided by the Johnston's organ. Clearly though, more research needs to be undertaken into the precise properties and function of the scolopidia. We have also assumed an idealized geometry of the Johnston's organ. In truth, the rigid prong in each radial slice is highly curved, which can lead to some of the outer scolopidia resisting rather than enhancing oscillatory motion.

Perhaps the most important omission from our current model is that we do not attempt to model the neural output from the scolopidia, although an important assumption of the integrate-and-twitch model is that neurons do not control scolopidia. This is a reasonable assumption due to the physiology of the Johnston's organ: each scolopidia is formed by the scolopele (the capsule containing the dynein filament) and an underlying neuron; the way in which synapses are positioned, though, suggests that a mechanical compression in the scolopele is sensed by the neuron and transmitted downstream to the brain, but not the other way around. Thus, we might assume that a charging event and subsequent "twitch" is concomitant with the firing of a neural pulse. In fact, under this hypothesis, the model sheds light on the sequence of neural firings within a particular radial slice: the outer scolopidia fire first, and the inner ones only fire during large oscillatory responses. Moreover, during large amplitude motion, the outer scolopidia may fire more than once. These hypotheses are currently being tested experimentally through synchronous recordings of neural signals and antenna motion.

In Section 3, based on our synthesis of earlier micro-mechanical models we introduced a longitudinally coupled cochlea model that includes many aspects of the cochlea mechanism already pointed out by others. In particular, we argue that it is the combination of spatial feed-forward, longitudinal coupling, somatic motility and a nonlinear transduction channel open probability that enables our model to find good qualitative and quantitative agreement with the compressive cochlea dynamics. Future work will further refine this model, considering different forms of longitudinal coupling and more realistic ion channel modelling. We will also present elsewhere evidence that the model captures the features of observed spontaneous otoacoustic emissions, the constant low-volume singing that can be output from live mammalian ears.

Note that this modelling success is found by physiological modelling without assuming a priori that the hair bundles are tuned to undergo a local bifurcation.

This finding seems to run counter to some current opinion in the literature which suggests the normal form for a Hopf bifurcation is a suitable phenomenological local model for the mammalian cochlea [21]. Indeed, proponents of a Hopf bifurcation hypothesis point to a supposed 1/3-power law in the amplification data. In fact it can be shown by harmonic balance [36] that a 1/3-power law comes from the presence of a cubic nonlinearity, which via Taylor expansion will always be present as the dominating nonlinear term in a smooth, symmetric, weakly nonlinear theory.

To compare both modelling studies it is helpful to note the contrasting complexity of the cochlea to that of the Johnston's organ. In the insect, there is a direct transduction of sound pressure waves in air into mechanical motion and thence to neural signals. This, combined with nonlinear compression, enables both an extreme sensitivity to low sound pressure levels and acute direction sensitivity. For mammals, evolution has had to work much harder in order to achieve the same level of sensitivity. It would seem that because mammals evolved from sea creatures whose sensory organs work underwater, the sensing has evolved to work within a fluid-filled tube. Thus subsidiary mechanisms are required in order to impedance match the air waves to fluid waves. One price to pay for this design solution is the loss of direction sensitivity. Also, much extra complexity is required in order for the OC to achieve a similar level of sensitivity to low sound levels. The advantage, though, of the mammalian configuration is the ability to accurately distinguish frequency.

It is also interesting to note the approach taken in both of these modelling case studies. In each case we have tried to distinguish between a purely phenomenological model, a more physiologically accurate model, and a simplified model that is derived from the physiological model via a rational, checkable process. For the insect, we considered first a phenomenological Ginzburg–Landau model, before going back to a basic physiologically inspired model. This was then further simplified via homogenization in order to derive a new lumped-parameter model, which is rather more akin to a van der Pol oscillator. For the cochlea, the situation is more complex. There are a large variety of different models in the literature, and in this paper we do no more than provide a glimpse of how the theory is progressing, with a clear bias towards our own work. Nevertheless, we have tried to steer a path between purely phenomenological models such as the Hopf bifurcation normal form and three-dimensional fluid-structure interaction models that aim to be anatomically accurate without necessarily capturing the true physiological processes.

As we move into the second decade of the 21st century, there is an increasing realization of the wide frontier that applied mathematics faces with the biological domain. As we begin to gaze into yet more complex biological systems, and more and more quantitative data becomes available, it is time perhaps to focus on what makes a "good" mathematical model. We must not forget the experience gained from the previous century when the physical world was the main focus of applied mathematics. The key is that a model should be, as far as possible, based on experimentally checkable hypotheses. It should aim to capture the essence of the true physics, and be both extensible and simplifiable. Attempts to "model everything" can produce

models with fancy graphical outputs that look realistic, but often rely on the fitting of many parameters and on hidden (unrealistic) physical assumptions. Above all, a good model should be developed in parallel with experimental results. It should be based on the experimental measurements, involve as few uncheckable "fitting parameters" as possible, and it should be able to predict the outcome of future experiments. Indeed, the model should suggest new hypotheses that are experimentally checkable, and if a hypothesis proves false, the model should be sufficiently adjustable to come up with a new explanation. This is, after all, the essence of the scientific method.

Acknowledgements

This paper is based on the plenary talk given by the first author at the ANZIAM conference in Queenstown in February 2010. He is grateful to the organizing committee and to the University of Auckland for additional financial support (and to Andrew Bassom, for his patience in waiting for the submission of this paper more than a year after the event). The research has been supported by grants from the UK EPSRC and BBSRC. The authors would like to thank their experimental collaborators on the research described herein: Helen Kennedy, Katie Lucas, Joe Jackson, Daniel Robert and James Windmill, all at the University of Bristol, and Nigel Cooper at the University of Keele. The theoretical work has also benefited from collaboration with Tom Irvine, Joe Jackson and Krasimira Tsaneva-Atanasova at the University of Bristol, and Dáibhid Ó Maoiléidigh at Rockefeller University.

References

[1] J. Ashmore et al., "The remarkable cochlear amplifier", *Hear. Res.* **266** (2010) 1–17; doi:10.1016/j.heares.2010.05.001.

[2] J. A. Assad and D. P. Corey, "An active motor model for adaptation by vertebrate hair cells", *J. Neurosci.* **12** (1992) 3291–3309.

[3] D. Avitabile, M. Homer, A. R. Champneys, J. C. Jackson and D. Robert, "Mathematical modelling of the active hearing process in mosquitoes", *J. Roy. Soc. Interface* **7** (2010) 105–122; doi:10.1098/rsif.2009.0091.

[4] G. Békésy, *Experiments in hearing* (McGraw-Hill, New York, 1960).

[5] C. de Boor and B. Swartz, "Collocation at Gaussian points", *SIAM J. Numer. Anal.* **10** (1973) 582–606; doi:10.1137/0710052.

[6] W. E. Brownell, C. R. Bader, D. Bertrand and Y. de Ribaupierre, "Evoked mechanical responses of isolated cochlear outer hair cells", *Science* **227** (1985) 194–196; doi:10.1126/science.3966153.

[7] N. P. Cooper and W. S. Rhode, "Nonlinear mechanics at the apex of the guinea-pig cochlea", *Hearing Res.* **82** (1995) 225–243; doi:10.1016/0378-5955(94)00180-X.

[8] P. Dallos, "Cochlear amplification, outer hair cells and prestin", *Current Opinion Neurobiol.* **18** (2008) 370–376; doi:10.1016/j.conb.2008.08.016.

[9] P. Dallos, "Prestin-based outer hair cell motility is necessary for mammalian cochlear amplification", *Neuron* **58** (2008) 333–339; doi:10.1016/j.neuron.2008.02.028.

[10] E. J. Doedel, H. B. Keller and J. P. Kernévez, "Numerical analysis and control of bifurcation problems, part II: bifurcation in infinite dimensions", *Int. J. Bifur. Chaos Appl. Sci. Engrg.* **1** (1991) 745–772; doi:10.1142/S0218127491000555.

[11] V. M. Eguíluz, M. Ospeck, Y. Choe, A. J. Hudspeth and M. O. Magnasco, "Essential nonlinearities in hearing", *Phys. Rev. Lett.* **84** (2000) 5232–5235; doi:10.1103/PhysRevLett.84.5232.

[12] S. J. Elliott, E. M. Ku and B. Lineton, "Time domain model of a nonlinear inhomogeneous cochlea"', in: *Concepts and challenges in the biophysics of hearing* (eds N. P. Cooper and D. T. Kemp), (World Scientific, Singapore, 2009) 74–81.
[13] G. Frank, W. Hemmert and A. W. Gummer, "Limiting dynamics of high-frequency electromechanical transduction of outer hair cells", *Proc. Natl. Acad. Sci. USA* **96** (1999) 4420–4425; doi:10.1073/pnas.96.8.4420.
[14] C. D. Geisler, "A realizable cochlear model using feedback from motile outer hair cells", *Hearing Res.* **68** (1993) 253–262; doi:10.1016/0378-5955(93)90129-O.
[15] R. Ghaffari, A. J. Aranyosi and D. M. Freeman, "Longitudinally propagating traveling waves of the mammalian tectorial membrane", *Proc. Natl. Acad. Sci. USA* **104** (2007) 16510–16515; doi:10.1073/pnas.0703665104.
[16] M. C. Göpfert and D. Robert, "Motion generation by Drosophila mechanosensory neurons", *Proc. Natl. Acad. Sci. USA* **100** (2003) 5514–5519; doi:10.1073/pnas.0737564100.
[17] J. Guckenheimer and P Holmes, *Nonlinear oscillations, dynamical systems and bifurcations of vector fields*, Volume 42 of *Applied mathematical sciences* (Springer, New York, 1986).
[18] H. Helmholtz, *On the sensation of tone* (Dover, New York, 1863).
[19] A. Hubbard, "A traveling-wave amplifier model of the cochlea", *Science* **259** (1993) 68–71; doi:10.1126/science.8418496.
[20] A. J. Hudspeth, "Making an effort to listen: mechanical amplification in the ear", *Neuron* **59** (2008) 530–545; doi:10.1016/j.neuron.2008.07.012.
[21] A. J. Hudspeth, F. Jülicher and P. Martin, "A critique of the critical cochlea: Hopf – a bifurcation – is better than none", *J. Neurophysiology* **104** (2010) 1219–1229; doi:10.1152/jn.00437.2010.
[22] J. C. Jackson and D. Robert, "Nonlinear auditory mechanism enhances female sounds for male mosquitoes", *Proc. Natl. Acad. Sci. USA* **103** (2006) 16734–16739; doi:10.1073/pnas.0606319103.
[23] J. C. Jackson, J. F. C. Windmill, V. G. Pook and D. Robert, "Synchrony through twice-frequency forcing for sensitive and selective auditory processing", *Proc. Natl. Acad. Sci. USA* **106** (2009) 10177–10182; doi:10.1073/pnas.0901727106.
[24] F. Jülicher, D. Andor and T. Duke, "Physical basis of two-tone interference in hearing", *Proc. Nat. Acad. Sci. USA* **98** (2001) 9080–9085; doi:10.1073/pnas.151257898.
[25] K. D. Karavitaki and D. C. Mountain, "Evidence for outer hair cell driven oscillatory fluid flow in the tunnel of corti", *Biophysical J.* **92** (2007) 3284–3293; doi:10.1529/biophysj.106.084087.
[26] H. J. Kennedy, A. C. Crawford and R. Fettiplace, "Force generation by mammalian hair bundles supports a role in cochlear amplification", *Nature* **443** (2005) 880–883; doi:10.1038/nature03367.
[27] H. J. Kennedy, M. G. Evans, A. C. Crawford and R. Fettiplace, "Fast adaptation of mechanoelectrical transducer channels in mammalian cochlear hair cells", *Nature Neuroscience* **6** (2003) 832–836; doi:10.1038/nn1089.
[28] M. M. M. Lagarde, M. Drexl, V. A. Lukashkina, A. N. Lukashkin and I. J. Russell, "Determining the identity of the cochlear amplifier: electrical stimulation of the tecta mouse cochlea", in: *Concepts and challenges in the biophysics of hearing* (eds N. P. Cooper and D. T. Kemp), (World Scientific, Singapore, 2009) 106–112.
[29] M. B. Lesser and D. A. Berkley, "Fluid mechanics of the cochlea. Part 1", *J. Fluid Mech.* **51** (1972) 497–512; doi:10.1017/S0022112072002320.
[30] J. Lighthill, "Energy flow in the cochlea", *J. Fluid Mech.* **106** (1981) 149–213; doi:10.1017/S0022112081001560.
[31] J. Meaud and K. Grosh, "The effect of tectorial membrane and basilar membrane longitudinal coupling in cochlear mechanics", *J. Acoust. Soc. Am.* **127** (2010) 1411–1421; doi:10.1121/1.3290995.
[32] D. Ó Maoiléidigh and F. Jülicher, "The interplay between active hair bundle motility and electromotility in the cochlea", *J. Acoust. Soc. Am.* **128** (2010) 1175–1190; doi:10.1121/1.3463804.
[33] W. S. Rhode, "Basilar membrane mechanics in the 6–9 kHz region of sensitive chinchilla cochleae", *J. Acoust. Soc. Am.* **121** (2007) 2792–2804; doi:10.1121/1.2718397.

[34] M. A. Ruggero, N. C. Rich, A. Recio, S. S. Narayan and L. Robles, "Basilar-membrane responses to tones at the base of the chinchilla cochlea", *J. Acoust. Soc. Am.* **101** (1997) 2151–2163; doi:10.1121/1.418265.
[35] C. R. Steele and K.-M. Lim, "Cochlear model with three-dimensional fluid, inner sulcus and feed-forward mechanism", *Audiol. Neurotol.* **4** (1999) 197–203; doi:10.1159/000013841.
[36] R. Szalai, A. R. Champneys, M. Homer, D. Ó Maoiléidigh, H. J. Kennedy and N. P. Cooper, "On the origins of the compressive cochlear nonlinearity", *J. Acoust. Soc. Am.*, to appear.
[37] R. Szalai, B. Epp, A. R. Champneys and M. Homer, "On time-delayed and feed-forward transmission line models of the cochlea", *J. Mech. Mat. Struct.* **6** (2011) 557–568; doi:10.2140/jomms.2011.6.557.
[38] J. Tinevez, F. Jülicher and P. Martin, "Unifying the various incarnations of active hair-bundle motility by the vertebrate hair cell", *Biophysical J.* **93** (2007) 4053–4067; doi:10.1529/biophysj.107.108498.
[39] J. Zheng, W. Shen, D. Z. Z. He, K. B. Long, L. D. Madison and P. Dallos, "Prestin is the motor protein of cochlear outer hair cells", *Nature* **405** (2000) 149–155; doi:10.1038/35012009.
[40] G. Zweig, "Finding the impedance of the organ of corti", *J. Acoust. Soc. Am.* **89** (1991) 1229–1254.
[41] J. Zwislocki, "Theorie der schneckenmechanik: qualitative und quantitative analyse", *Acta Oto-Laryngologica* **72** (1948) 1–76.